Two-Dimensional Crystals of Photosystem II: Biochemical Characterization, Cryoelectron Microscopy and Localization of the D1 and Cytochrome b559 Polypeptides

Kathleen M. Marr,* David N. Mastronarde,‡ and Mary K. Lyon*

*Department of Molecular, Cellular and Developmental Biology, and ‡Boulder Laboratory for 3D Fine Structure, University of Colorado, Boulder, Colorado 80309-0347

Abstract. Photosystem II (PS II) is a photosynthetic reaction center found in higher plants which has the unique ability to evolve oxygen from water. Several groups have formed two-dimensional PS II crystals or have isolated PS II complexes and studied them by electron microscopy and image analysis. The majority of these specimens have not been well characterized biochemically and have yielded relatively low resolution two-dimensional projection maps with a variety of unit cell sizes.

We report the characterization of the polypeptide and lipid content of tubular crystals of PS II. The crystals contain the reaction center core polypeptides D1, D2, cytochrome b559, as well as the chlorophyll-binding polypeptides (CP) CP47, CP43, CP29, CP26, CP24, and CP22. The lipid composition was similar to the lipids found in the stacked portions of thylakoids. We also report a 2.0-nm resolution projection map determined by electron microscopy and image analysis of frozen, hydrated PS II crystals. This projection map includes information on the portion of the complex buried in the lipid bilayer. The unit cell is a dimer with unit vectors of 17.0 and 11.4 nm separated by an angle of 106.6°. In addition, F_{ab} fragments against D1 and cytochrome b559 were used to localize those two polypeptides, and thus the reaction center, within the PS II complex. The results indicate that D1 and cytochrome b559 are found within one of the heaviest densities of the monomeric unit.

Photosystem II (PS II)[1] converts light energy to chemical energy, splitting water in the process and releasing oxygen as a byproduct. Consequently, PS II is the major source of oxygen for the atmosphere. Multiple pigments and at least 13 major polypeptides make up PS II, which is found in the photosynthetic membranes of green plants (for review see Hansson and Wydrzynski, 1990; Staehelin and van der Staay, 1995). All but three of the polypeptides are intrinsic to the membrane. The three extrinsic polypeptides are found on the lumenal side of the membrane and are involved in oxygen evolution (for review see Ghanotakis and Yocum, 1990). The combined molecular mass of the polypeptides and pigments is ~350 kD. This figure does not include the eight very low molecular mass polypeptides known to be associated with PS II (Ikeuchi and Inoue, 1988; Schroder et al., 1988; Staehelin

and van der Staay, 1995). In addition, the stoichiometry of each polypeptide is not known with certainty, so the molecular mass of PS II can only be estimated.

Two of the core polypeptides of PS II (D1 and D2) have sequence homology with the two core polypeptides (L and M) of the *Rhodopseudomonas viridis* reaction center (Holschuh et al., 1984; Zurawski et al., 1984), so that the structure of D1 and D2 can be inferred from the structure of the *R. viridis* reaction center (Deisenhofer and Michel, 1989). However, PS II is more complex than the bacterial reaction center. There have been many efforts to determine the structure of PS II directly, including examination of isolated complexes (Irrgang et al., 1988; Dekker et al., 1990; Haag et al., 1990; Boekema et al., 1994, 1995). There are several reports of two-dimensional crystals of photosystem II being formed in thylakoids after detergent treatment (Seibert et al., 1987; Bassi et al., 1989; Holzenburg et al., 1993; Lyon et al., 1993; Santini et al., 1994), as well as one type of PS II crystal which occurs in barley mutants lacking some photosystem I polypeptides (Simpson, 1983; Miller and Jacob, 1991). Each crystal type appears to be unique. The unit cells have ranged from 17.8 × 26.7 nm to 11.5 × 16.1 nm (Bassi et al., 1989; Lyon et al., 1993, respectively). In addition, there is a conflict in the literature as to

---

1. *Abbreviations used in this paper:* CP, chlorophyll-binding polypeptide; cyt b559, cytochrome b559; LHC II, light-harvesting chlorophyll a/b complex associated with photosystem II; OEP, oxygen-evolving polypeptides; PS II, photosystem II.

whether PS II exists as a monomer (Holzenburg et al., 1993) or dimer (Seibert et al., 1987; Bassi et al., 1989; Miller and Jacob, 1991; Peter and Thornber, 1991; Lyon et al., 1993; Boekema et al., 1994, 1995; Santini et al., 1994). The crystals in all these studies are found in preparations that include large numbers of vesicles and membrane fragments, so that the exact composition of each crystal type is difficult to determine. This makes it difficult to compare structures derived from the various crystals, or even to interpret the structures and their functional significance with any degree of certainty. In this report, we have characterized the polypeptide and lipid content of tubular crystals of PS II (Lyon et al., 1993) and produced a projection map from frozen hydrated crystals. F_{ab} fragments were used to localize D1 and cytochrome b559 (cyt b559), thereby localizing the reaction center core to a specific density within the projection map.

Materials and Methods

Preparation of Samples

Market spinach was purchased locally. Greenhouse spinach was grown in soil under natural light conditions and was harvested approximately two months after planting. Two-dimensional crystals were prepared as in Lyon et al. (1993).

Biochemical Characterization

The samples were enriched for the tubular crystals by repeated, low speed centrifugation (5,000 rpm for 6 min, Eppendorf 5402 centrifuge) and monitored by electron microscopy for enrichment. Gel electrophoresis and immunoblotting were done as in Lyon et al. (1993) using 15% acrylamide mini-gels. Each lane was loaded with 1 µg of chlorophyll. Antibody binding was detected by an amplified alkaline phosphatase method (Bio-Rad, Hercules, CA). The antibodies used were: anti-D1 and -D2 (Dr. B. Diner, E.I. DuPont de Hemours & Company, Wilmington, DE; Nixon et al., 1990), anti-CP47 and -CP43 (Dr. S. Mayfield, Scripps Research Institute, La Jolla, CA), anti-cyt b559 (Dr. W. Cramer, Purdue University, West Lafayette, IN; Tae et al., 1988), anti-CP22 (Dr. C. Yocum, University of Michigan, Ann Arbor, MI; Bowlby and Yocum, 1993), anti-CP24 and -CP26 (Dr. L.A. Staehelin, University of Colorado, Boulder, CO; Falbel and Staehelin, 1992) and anti-CP29 (Dr. D. Simpson, Carlsberg Laboratory, Copenhagen, Demmark; Høyer-Hansen et al., 1988; Falbel and Staehelin, 1992).

Lipids were extracted and separated as in Jacob and Miller (1986). Grana membranes were prepared as in Berthold et al. (1981). Plates of silica gel with a fluorescent indicator (Sigma Chem. Co., St. Louis, MO) were examined by UV illumination, then stained with osmium tetroxide vapors before photographing (Kates, 1972).

Electron Microscopy

Labeling with Anti-CP24, CP26, and CP29. Freshly prepared, dilute sample was applied to glow-discharged, carbon-coated nickel grids. The grids were rinsed by floating on successive drops of distilled water and then on a drop of 1% fish gelatin (Amersham Corp., Arlington Heights, IL) in buffer (15 mM NaCl, 5 mM $MgCl_2$, 20 mM Tris, pH 7.5). After 2 min the grids were transferred to a drop containing either the test antibody, buffer, or non-immune serum (each diluted with 1% fish gelatin). CP24 and CP26 anti-sera were used at 1:20 dilutions while CP29 anti-serum was used at a 1:50 dilution. Control grids were made using non-immune rabbit serum (CP24 and CP26) or mouse serum (CP29) at the same dilutions. Grids were incubated in a humid chamber that had been placed on a magnetic stir plate so that the grids would rotate on top of the drop (Dr. T. Giddings, personal communication). After incubation for 0.25–3 h, the grids were washed by floating on drops of buffer for a total of 1 h. Each grid was incubated for 5 min on a drop of anti-IgG gold conjugate. Finally, the grids were washed by floating on buffer for 30 min, rinsed quickly in two drops of distilled water, and then stained with 2% uranyl acetate. Im-

ages were taken on a Philips CM10 electron microscope at magnifications of 13,500 and 25,000×.

Preparation of and Labeling with F_{ab} Fragment. Polyclonal serum containing IgG directed against the cyt b559 (last 12 residues of the COOH terminus, Tae et al., 1988) and the D1 (last 16 residues of the COOH terminus) polypeptides each were purified by passage over a protein A column (Pierce, Rockford, IL). F_{ab} fragments were generated from the purified IgG by digestion with papain according to the manufacturer's instructions (Pierce). F_c fragments and undigested IgG were removed by passage over a protein A column.

Purified F_{ab} fragments were assayed for binding activity using standard immunoblots (Lyon et al., 1993) and then tested on tubular crystals. Dilute sample containing tubular crystals of PS II was applied to glow-discharged, carbon-coated copper grids. The grids were rinsed by quickly floating on successive drops of buffer (15 mM NaCl, 5 mM $MgCl_2$, 20 mM Hepes, pH 7.5) and then on a drop of cytochrome c blocking solution (0.5 mg/mL in buffer, pH 7.5) for 2 min (Kubalek et al., 1987). The grids were transferred to a drop containing non-immune rabbit (Jackson ImmunoResearch Laboratories, Inc., West Grove, PA), anti-D1, or anti-cyt b559 F_{ab} fragments (1:10 in 0.5 mg/mL cytochrome c in buffer, pH 7.5). The grids were incubated for 15 min and then transferred to three successive drops of buffer for a total of 15 min. The grids were then floated for 5 min on a drop containing anti-rabbit IgG coupled to 10 nm gold. Finally, the grids were rinsed on two successive drops of distilled water and stained with 2% uranyl acetate.

For image processing, labeling with F_{ab} fragments was repeated as above, omitting the incubation with IgG-gold. Images were taken on a Philips CM10 in low dose mode at a nominal magnification of 39,000×.

Cryoelectron Microscopy

Samples were frozen in buffer as in Brisson and Unwin (1985), using 18.0-nm-thick carbon films (Arizona Carbon Foil Company, Tucson, AZ) on 400 mesh copper grids. Images were obtained on a Philips CM10 operated in low dose mode with a Gatan 626-MAN cryostage (Pleasanton, CA), operated at approximately −168°C. A 300-µm condenser aperture and 70-µm objective aperture were used. Two images of each tube were taken using low dose conditions. The first image was taken at a nominal underfocus of 300 nm and a second image was taken at 600 nm underfocus. The actual defocus values were determined as in Zhou and Chiu (1993) and were 268 nm and 980 nm underfocus.

General Image Processing

Images were processed with a hybrid of two approaches: correlation averaging using the SPIDER system (Frank and Goldfarb, 1980; Frank et al., 1981; Saxton and Baumeister, 1982) with appropriate modifications, and image alignment and comparison methods developed in the Boulder Laboratory for 3-D Fine Structure (Mastronarde et al., 1992). The major steps in the processing included obtaining average images from individual tubular crystals, aligning and density-scaling these averages to each other, and selecting the best of these final averages to combine into a grand average. Variations of these steps were required for processing images derived from frozen crystals and for comparing F_{ab} labeled to control samples, as detailed below.

Digitizing Images. Negatives were screened in a diffractometer. Tubular crystals displaying a reasonable diffraction pattern were digitized with a Star I cooled CCD camera (Photometrics Ltd., Tucson, AZ) connected to a MicroVax III computer (Digital Equipment Corporation, Maynard, MA). The optical density was measured at each pixel; the pixel size varied from 0.578 to 0.622 nm. Although the camera has a maximum frame size of only 572 × 378 pixels, the digitizing program was able to capture the image of an entire crystal in a series of two to four overlapping frames by using a motor-driven light box. A blending program assembled these frames into a single image (Mastronarde et al., 1993). To do so, it determined the match between adjacent frames in the region of their overlap and resolved any misalignment between them in a graded fashion over the course of 50 pixels. These misalignments were less than 1 pixel. To keep density gradients across the image from appearing in the final average, the digitized image was high-pass filtered. After digitizing, the remainder of the processing was done on a AXP 3000 computer (Digital Equipment Corporation).

Correlation Averaging. To obtain an initial starting reference for cross-correlation, a 256 × 256 pixel area was selected from the digitized image and Fourier transformed. Reflections in the power spectrum were indexed

using SPIDER routines, the transform masked to a 3 × 3 pixel area around each reflection, and the inverse transform taken. From this initial reference, a 64 × 64 pixel reference image was excised from the center. This reference image was cross-correlated with the original crystal image. The SPIDER peak search routine located peaks in the correlation. For each peak whose height was at least 60% of the maximum correlation, a 64 × 64 pixel window was excised from the corresponding location in the tubular crystal. These windows were averaged. This new reference average was low- and high-pass filtered and then used to find the appropriate alignment parameters for each previously located individual window. After determining the necessary alignments, a subset of windows was selected based on the amounts of rotation, translation, and a new strength of correlation between each aligned window and the reference average. A program was written to facilitate selection of these windows by allowing examination of the distribution of the three parameters. Typically, windows were retained if their rotations were less than 4°, their displacements less than 1.5–2 pixels, and their new correlation strength at least 40–50% of the new maximum correlation. Each selected window was rotated and translated into alignment with respect to the reference average with a single quadratic interpolation; the final average and variance images were then computed.

Alignment, Scaling, and Combination of Final Averages to Obtain a Grand Average. The final averages from individual tubular crystals were aligned to each other with linear transformations (Mastronarde et al., 1992). This method eliminated minor differences among the averages in unit cell dimensions and angles that can arise from small variations in magnification or specimen tilt. Initially, the reference for alignment was either one of the final averages or a grand average of several final averages from a previous analysis. However, once a grand average of aligned images was obtained, the procedure was reiterated with that as reference. The alignment program measured the difference between the transformed individual average and the reference image and used a simplex algorithm (Press et al., 1989) to search for transformation parameters that minimized the difference. After an alignment transformation was found, the aligned image was rotated by 180°, the shift was found that would align the rotated image to the reference, and half of this shift was added to the alignment transformation so that the 180° rotation of the final aligned image would be equally well aligned to the reference.

After alignment, the densities in each image were scaled to match those in some reference image, initially the grand average of unscaled images and then, on a second iteration, the average of scaled images. Because linear scaling would not have been adequate in some cases, a more general mapping was used. To implement this, pixels were divided into 10 sets based on their density levels in the reference image, and average density values were determined for each set of pixels. A smooth curve of density in the reference versus density in the image being scaled was generated by locally weighted regression on these average densities (Wand and Jones, 1995). Using this curve, the density value at any particular pixel could then be mapped to a value in the reference image. Variances were scaled by the square of the slope of a line fit to all 10 average densities.

Analysis of Images of Frozen Crystals

Three modifications were required to obtain quality averages from the frozen, hydrated samples. First, alignment of individual windows from a 300-nm defocus image was difficult because of the low contrast of these images. Therefore, the 300- and 600-nm images of each crystal were combined for initial processing. The two images were digitized in approximate registration. A matrix of local displacements between the two images was obtained by cross-correlation in a series of local patches (96 × 96 pixels). From these displacements, a linear transformation was obtained to align the 600-nm image with the 300-nm image. The 300-nm and transformed 600-nm images were then added together. The contrast on all images was reversed.

Second, the initial cross-correlation map from each tubular crystal contained peaks displaced by half a unit cell. Therefore, to obtain an initial set of averages, correlation peaks were selected by hand from each crystal to ensure that all peaks were from the same lattice.

The third modification was to reiterate the cross-correlation. This was done by combining averages from several tubular crystals to form a grand average. An individualized reference was generated for each crystal by applying the inverse of the transformation needed to align a preliminary average from one side of that crystal to the grand average. With a grand average as reference, the SPIDER automatic peak search reliably found peaks that were not displaced by half a unit cell. As new grand averages

became available, they were used to obtain improved references. The reiteration increased the number of high quality windows. Each individualized reference was flipped about its *x* axis to extract windows from the opposite side of the tubular crystal.

The peak positions and alignment shifts and rotations obtained from the combined 300- and 600-nm images were then applied to the 300-nm images to obtain final averages from each crystal. Averages were selected for combination into a grand average so as to maximize the resolution. Resolution was assessed by the spectral signal-to-noise ratio (Unser et al., 1987), using the averages from each side of the crystals, not individual windows, as the elements of the analysis.

Analysis of Antibody Labeled Crystals

Images from both labeled and control crystals were processed as described above. Additional procedures included: (a) final alignment of averages using the central unit cell of each average, (b) selection of subsets for obtaining grand averages, and (c) statistical comparisons between F_{ab}-labeled and control averages.

Final Alignment Using Single Unit Cell. Even after the alignment of 64 × 64 pixel averages, the structure inside the unit cells within each final average showed subtle shape changes from one final average to another. To reduce these variations as much as possible for the antibody-labeled material, we aligned just a single unit cell from each average. For each aligned average and for the reference, the average was linearly transformed so that just the central unit cell occupied a 24 × 32 pixel rectangle. Linear alignment transformations were found for each rectangularized average. These transformations were used to modify the transformations from the full-image alignment procedure, so that newly aligned unit cell images could be obtained with a single interpolation.

Selection of Averages. To obtain grand averages for both the F_{ab} labeled and control crystals, averages from each crystal were selected by two methods. First, the noisiest averages originating from a particular grid were eliminated if they degraded the resolution of the grand average for that grid. Resolution was assessed by the spectral signal-to-noise ratio (Unser et al., 1987).

Second, a smaller subset of final averages was defined by eliminating ones with particularly distorted unit cells, as was done by Guo et al. (1995). The degree of distortion was assessed from the a/b ratio and the unit cell angle. These parameters were derived from the transformation needed to align a particular final average to the reference grand average.

Statistical Comparisons. Before statistical comparisons were made, averages were filtered to a resolution of 2.0 nm and twofold symmetry was imposed. Comparisons between antibody-labeled and control images were done with a two-level nested analysis of variance (Sokal and Rohlf, 1981; Mastronarde et al., 1992). This analysis can test for differences between samples of different kinds while simultaneously taking into account both variability among the samples of a given kind and variation in the elements contributing to each individual sample. In initial tests, the samples were the individual windows, and the scaled final averages and variance maps were used in the analysis of variance (just as in Mastronarde et al., 1992). However, when samples of the same kind but from different grids were compared, there were statistically significant differences between grids. Thus, another level of variability (among grids) needed to be taken into account in the statistical analysis. To do so with a two-level analysis, the individual final averages were considered as samples. The simple mean and standard deviation of filtered final averages from each grid were used in the analysis of variance. This analysis accounted for both the variation among the final averages from one grid and the variation among the grids of one type.

Results

Sequential detergent treatments of spinach thylakoids under specified conditions (Lyon et al., 1993) yield tubular two-dimensional crystals of photosystem II (Fig. 1 a, inset). Preparations which were highly enriched for the tubular crystals (Fig. 1 a) were used for determining the polypeptide and lipid composition of these crystals. Antibodies were used to detect individual polypeptides by comparing immunoblots of whole thylakoids and crystal preparations (Fig. 1 b). The results showed a high degree of enrichment
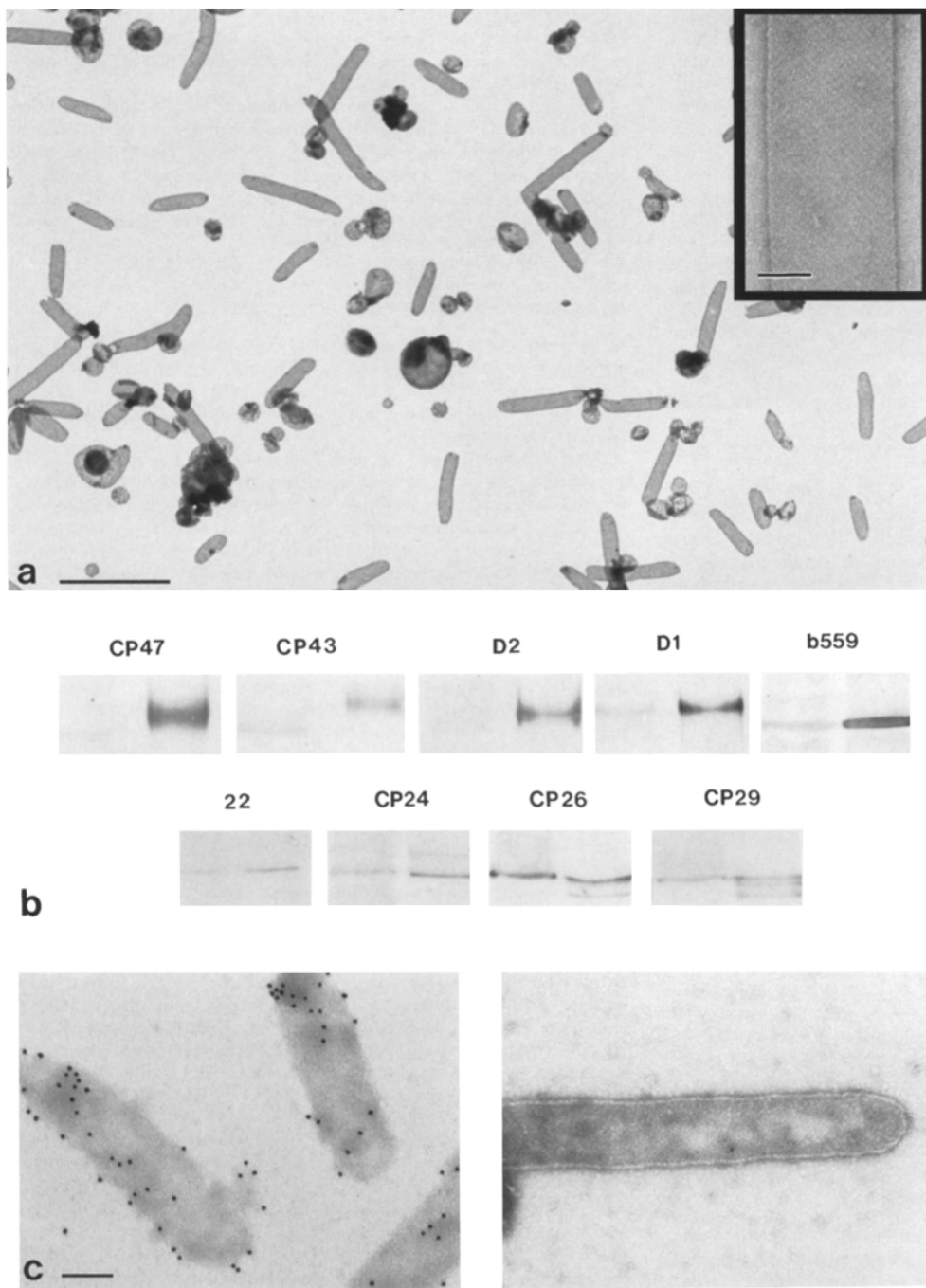
Figure 1. Biochemical characterization of the tubular crystals. (*a*) A preparation used for immunoblot analysis, showing the high degree of enrichment for the crystals. (*Inset*) Higher magnification image of a single, negatively stained crystal. (*b*) Immunoblot analysis. The left hand lanes of each pair are whole thylakoids, while the right hand lanes are tubular crystals. Pair 1, anti-CP47; pair 2, anti-CP43; pair 3, anti-D2; pair 4, anti-D1; pair 5, anti-cyt b559; pair 6, anti-CP22; pair 7, anti-CP24; pair 8, anti-CP26; pair 9, anti-CP29. (*c*) Antibody labeling was done to confirm the presence of CP24, CP26, and CP29, using gold-labeled secondary antibodies to detect the primary antibodies. The first panel is an example of a tubular crystal labeled with anti-CP24 and the second panel is a control. Results are tabulated in Table I. Bars: (*a*) 1 μm; (*a, inset*) 100 nm; (*c*) 125 nm.

for D1, D2, CP47, CP43, cyt b559, and CP22. However, CP24, CP26, and CP29, while present in the preparations, did not show the same degree of enrichment as the core polypeptides. To determine more definitely the presence or absence of CP24, CP26, and CP29 in the crystals, direct labeling was done with antibodies specific for each polypeptide (for example see Fig. 1 *c*). The specific antibodies were detected with secondary antibodies conjugated with gold. A Student's two-tailed *t*-test was used to compare the means of labeled versus control samples. The significance levels (Table I) were quite high, indicating that CP24, CP26, and CP29 were included in the crystals.

The lipid composition of the crystals was examined by thin-layer chromatography (Fig. 2, lane *3*) and compared to a grana preparation (Fig. 2, lane *2*). A grana membrane preparation was used for the comparison because PS II is found almost exclusively in the grana region of thylakoids and it has previously been shown that the lipid populations of granal and stromal regions of thylakoids are different (for review see Murphy, 1986). The crystal preparation had a lipid profile very similar to the grana preparation. However, there was a slight enrichment for two minor bands in the crystal preparation (Fig. 2, *arrows*). One of these bands (*lower arrow*) can be tentatively identified as consisting of diphosphatidyl glycerol and sulphoquinovosyl diacylglycerol, based on relative mobilities (Kates,

	Crystals counted	Total area surveyed	Mean, gold particles per crystal	Standard deviation	Significance level*
		μ^2			
α-CP26	11	2.3	8.5	5.2	98%
α-CP24	8	1.9	21.1	8.7	99%
rabbit serum	10	1.9	3.1	3.0	
a-CP29	29	5.4	7.9	4.5	99%
mouse serum	31	6.2	4.2	3.2	

Note: A variance ratio test was performed. The variances within each set were statistically equivalent.
*Walpole and Mayers, 1978.

1972; Rawyler and Siegenthaler, 1980). The smaller band (*upper arrow*) has been detected in thylakoids (Kates, 1972) but has not been identified.

Projection Maps: Cryoelectron Microscopy

Tubular crystals were imaged after freezing over carbon films (Fig. 3 *a*). At the defocus level shown (980 nm underfocus), the dark unit cells and the light grooves are faintly visible. Bulbous ends were frequently found on the crystals, but completely formed tubular crystals were more typical. Contrast was reversed before image analysis so that the protein would be light and the results would be comparable to negatively stained samples. The log of the power spectrum from one area of the tube is shown in Fig. 3 *b*. Reflections from both sides of the tube are clearly visible. Some of the reflections were quite close together (*arrows*). The close reflections are related to the orientation of the lattice with respect to the tube axis, as in Brisson and Unwin (1984). It was possible to find areas where these reflections were sufficiently far apart to be separated by the use of a small mask. An initial reference was then obtained (Fig. 3 *b*, *inset*) and was used for cross-correlation and selection of the best areas of each crystal. From the best areas, individual averages were obtained from
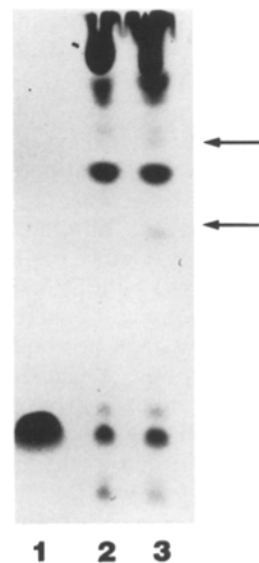

Figure 2. Thin layer chromatography of lipids. Lane *1*, Purified digalactosyl diacylglycerol. Lane *2*, Grana membranes. Lane *3*, Tubular crystals. The lipid profiles in lanes *2* and *3* are very similar. Two bands (*arrows*) appear to be slightly more concentrated in the crystal preparations. Dark areas at the top of the plate are pigments.

each crystal (example, Fig. 3 *c*) and combined to form a grand average. Cross-correlation with this grand average was reiterated, selection and rotational and shift corrections were repeated to obtain an improved average from each crystal. The final projection map included 1053 windows and is shown in Fig. 4. Windows were 64 × 64 pixels, the same size as the reference (Fig. 3 *b*, *inset*). Only windows requiring no more than 4° of rotational correction or 0.87-nm shift correction were included.

The final projection map (Fig. 4) shows a high degree of twofold symmetry about a central cleft. The correlation coefficient was 0.98 for this density map and its 180° rotation after filtering to 2.0 nm resolution. The density map in Fig. 4 *a* has not been filtered, nor has symmetry been imposed. The two areas showing the greatest difference in symmetry are marked by arrows. While the difference is subtle, it appears that one-half of the dimer has a heavier density in this region. This subtle difference was apparent in the averages from individual crystals and was taken into account when individual averages were combined to form the grand average shown in Fig. 4 *a*. Because the differences were so subtle, twofold symmetry was imposed for all further work. The spectral signal-to-noise ratio was 3 at 2.05 nm, 2 at 2.01 nm, and 1 at 1.83 nm. Therefore, the useful data extends to at least 2.0 nm. The contour plot (Fig. 4 *b*) has been filtered to 1.7 nm and twofold symmetry imposed. The unit cell is 11.4 × 17.0 nm.

There are several features of note. First, the unit cell clearly consists of a dimer. Each half of the dimer includes roughly four areas, indicated as A, B, C, and D on the contour map (Fig. 4 *b*). The heaviest densities are A and B. C is a low density area extending from A and B. The D area is somewhat separate, being connected to the B area by low density material. The crystallographic connections between the unit cells (arrows) are only between the low density areas (D and C) whereas the high density A and B areas of the two monomers are in relatively close proximity around the center of the unit cell.

The potential volumes of each area were determined (Table II). Densities were integrated over each area after subtracting the background density (darkest part of the grooves). Integrals are expressed as a percentage of the integral of the monomer (Table II). Integrals were converted to volumes by assuming that the six pixels of the densest area (which had an integral of 6.1% of the monomer) had a thickness of 9.45 nm. This value is midway between the thickness determined by low-angle shadowing of the crystals (Lyon et al., 1993) and the maximum thickness of negatively-stained isolated PS II particles (Boekema et al., 1995). The volume was converted to potential mass using the value of 1.05 kD/nm³ (Kühlbrandt, 1987). Of particular interest is the potential mass of one half of the dimer (the monomer). The mass of a single copy of each of the polypeptides known to be in the crystals (Fig. 1 *b*) is 270 kD, not including chlorophyll or other pigments. The monomer has sufficient volume for a mass of ∼332 kD.

Localization of the D1 and cyt b559 Polypeptides

Negatively stained tubular crystals, typical of those used for F_{ab} fragment labeling, are shown in Fig. 5, *a* and *b*. Experimental conditions, including type of blocking agent,
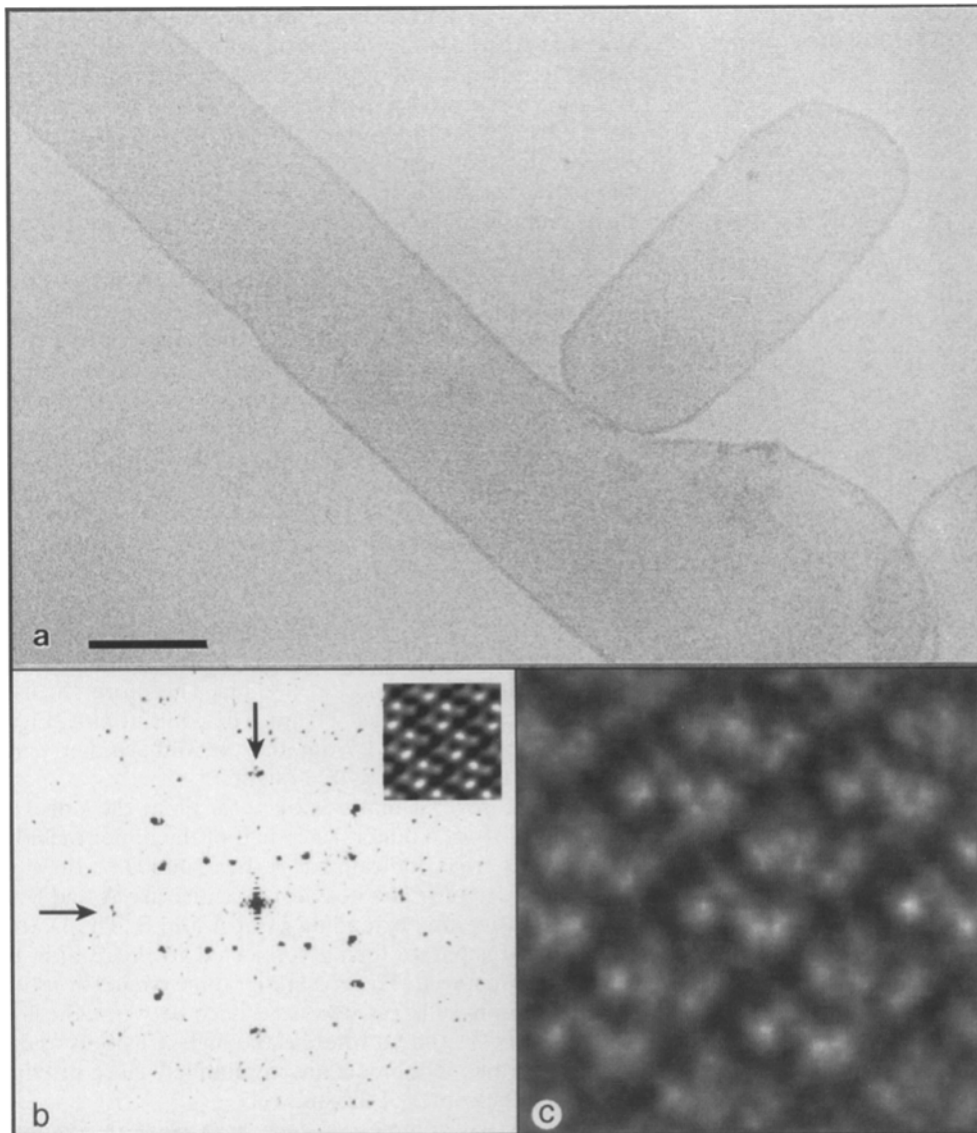
Figure 3. (*a*) Electron micrograph of frozen, hydrated crystals. Defocus value = 980 nm. The protein is dark, while lipid and ice are light. Ordered areas are just barely visible, particularly if the micrograph is viewed at a glancing angle. (*b*) Log of the power spectrum from a portion of the larger tubular crystal in *a*. Diffraction from both sides of the crystal are visible. A very small mask size was required to separate closely spaced reflections (*arrows*). (*Inset*) Example of an initial reference obtained from masked diffraction patterns. (*c*) An example of a preliminary projection map obtained from one side of a single crystal. Bar, 140 nm.

incubation times, and antibody concentration were determined empirically to avoid excessive labeling (Fig. 5 *c*) and consequently an obscured diffraction pattern.

To ensure adequate sampling of the data, three grids were used for each sample (D1, cyt b559, and control). There was a total of 22 crystals (4271 64 × 64 windows) for the control samples, 27 crystals (5555 windows) for the D1 labeled sample, and 20 crystals (3759 windows) for the cyt b559 labeled sample. Each set of data yielded a grand average image of the PS II complex. The density map shown (Fig. 6 *a*) is the grand average of the samples from one control grid. The map is similar to the average from negatively stained PS II tubular crystals shown in Lyon et al. (1993). The significant difference between the grand average image from complexes labeled either with anti-D1 F_{ab} fragment or with cyt b559 F_{ab} fragment and the grand average image from control samples clearly shows the location of the F_{ab} fragment and therefore of the polypeptide being probed. In Fig. 6, *b* and *c*, differences not significant at the 0.05 level have been set to zero (*gray*). The most significant pixel in the D1 projection map (P =

0.0027, Fig. 6 *b*) indicates that the D1 polypeptide is located in density A. The next most significant pixel in this map has a P = 0.007. In the cyt b559 difference projection map (Fig. 6 *c*), the most significant pixel is also in density A, near the D1 polypeptide, but closer to the center of the complex. Here, the two most significant pixels have P = 0.007 and P = 0.0038; the next most significant pixel in the map has a P = 0.016. Note that the most significant pixel in each case is part of a group of pixels with significant differences between labeled and control images. The spatial relationship between the two polypeptides is more easily seen in Fig. 6 *d* which shows the locations of both D1 and cyt b559 on a contour map of the PS II complex. These results are from a subset of 62 averages obtained by eliminating noisy averages that reduced resolution. A similar, but weaker, pattern of differences was obtained from a smaller subset of averages selected by including only those averages with an a/b ratio of 0.738–0.712 and angles of 103.5–106.1°. In addition, the difference between the D1 average and the sum of cyt b559 and control averages, and between the cyt b559 average and the sum of D1 and con-

Region	Pixels	Integrated density	Potential mass
		% of monomer	kD
monomer	178	100	332
A	15	13.7	45
B	13	11.4	38
A,B and surrounding area	43	34.9	116
C	5	3.1	10
D	25	17.9	59

Based on a height of 9.45 nm at the highest point (Lyon et al., 1993; Boekema et al., 1995) and a density of 1.05 kD/nm³ (Kühlbrandt, 1987).

trol averages was computed; these differences showed a similar pattern for both subsets of averages.

Discussion

Composition of Tubular Crystals

Previous work using gel electrophoresis and immunoblots (Lyon et al., 1993) has shown that tubular crystals of PS II contained neither the light-harvesting chlorophyll a/b complex associated with photosystem II (LHC II) nor the three extrinsic polypeptides associated with oxygen evolution. However, the absorption spectrum suggested that pigments normally associated with PS II were included in these crystals. In this work, the composition of the tubular PS II crystals has been determined. All major polypeptides were present: D1, D2, CP47, CP43, CP22, and cyt b559. In addition, the minor antennae polypeptides of CP29, CP26, CP24, and CP22 were present. These results do not exclude the possibility that other polypeptides, particularly the 10-kD (Ljungberg et al., 1986) and other small polypeptides, are also present. The lipid content appeared to be very similar to the lipid content of grana membranes, which is particularly significant because lipid has been implicated in maintaining both the structure (Jacob and Miller, 1986) and function of PS II (Gounaris et al., 1983; Siegenthaler et al., 1987).

Previous structural work with PS II has produced a variety of two-dimensional crystals with differing unit cell sizes: 16.8 × 18.9 nm (Holzenburg et al., 1993), 17.8 × 26.7 nm (Bassi et al., 1989), 18.0 × 26.0 nm (Santini et al., 1994), 16.0 × 23.5 nm (Simpson, 1983; Miller and Jacob, 1991), and 17.5 × 20.4 nm (Seibert et al., 1987). The larger sizes from other crystal types may result from varying amounts of lipid and/or detergent associated with each unit cell. However, it is also quite likely that much of the variation comes from differences in polypeptide content. Gel electrophoresis of two crystal preparations showed LHC II as the most prominent component (Bassi et al., 1989; Holzenburg et al., 1993). Isolated particles of purified spinach PS II complexes were 9.7 × 17.2 nm, while PS II-LHC II complexes were 12.3 × 26.8 nm (Boekema et al., 1995). The PS II complexes in the tubular crystals are clearly too small to include LHC II.

Structure: Interpretation of the Unit Cell

Freeze-etch work with grana membrane fragments has established that PS II particles have a tetrameric appearance
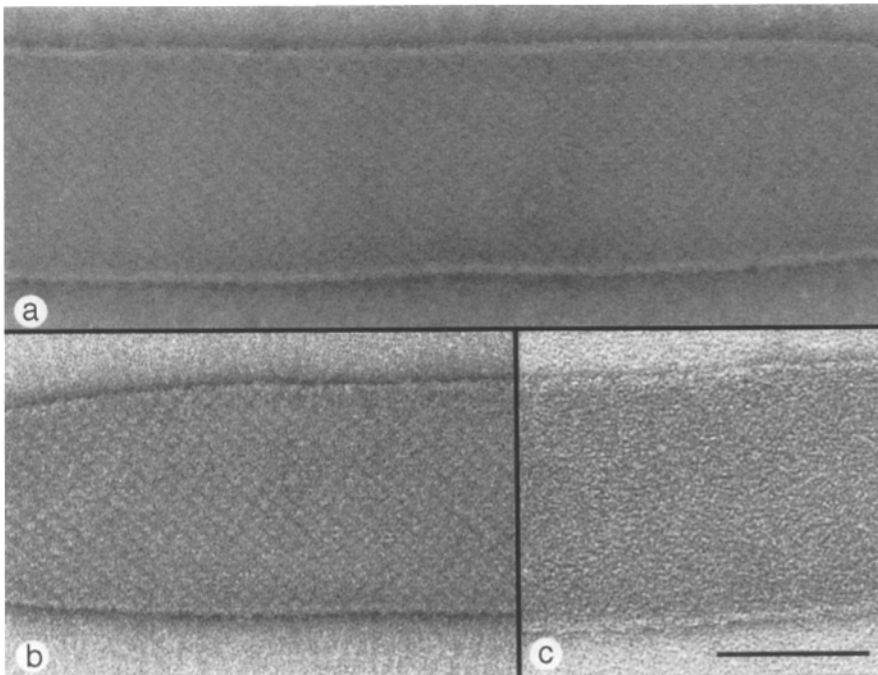
Figure 4. (a) Density map of the average obtained from the 268 nm defocus images. Symmetry has not been imposed, nor has this average been filtered. The high degree of twofold symmetry is clearly evident. Slight asymmetry was consistently noticed in the areas indicated with arrows. (b) Contour map with no symmetry imposed, filtered to 1.7 nm, for comparison with the symmetrized contour map (c). (c) Contour map of the average after filtering to 1.7 nm. Twofold symmetry has been imposed. The unit cell was 11.4 × 17.0 nm. Individual areas of density within the monomeric unit are indicated by A–D. Arrows indicate crystallographic connections between the unit cells.

Figure 5. Electron micrograph of negatively stained crystals of PS II. Nominal defocus value = 300 nm. Protein complexes are white. (*a*) Control. (*b*) Anti-D1 labeled. (*c*) Crystal excessively labeled with anti-D1 F_{ab}. Ordered areas are no longer visible. Bar, 120 nm.

on the lumenal face of thylakoids (for recent work, see Simpson and Andersson, 1986; Seibert et al., 1987). When the oxygen-evolving polypeptides (OEPs) are removed, these particles appear dimeric (Seibert et al., 1987). Similar changes from tetramers to dimers upon removal of the OEPs have been reported with two-dimensional crystals of PS II (Bassi et al., 1989; Santini et al., 1994). The unit cell of the tubular crystals in this report had a dimeric appearance, twofold symmetry and lacked the OEPs. Based partially on this, we have concluded that the unit cell consists of two PS II complexes and corresponds to the PS II particles observed in grana membranes after the OEPs have been removed. The monomer within each unit cell would thus correspond to a single PS II complex.

There has been a report of a two-dimensional crystal consisting of monomeric units of PS II (Holzenburg et al., 1993). The surface layers of the unit cell appeared tetrameric, but at levels of the reconstruction which corresponded to membrane-internal portions, the unit cell was monomeric in appearance (Holzenburg et al., 1993). The authors concluded that PS II in the native membrane consists of monomeric units, not dimers. However, both the crystal and the diffraction pattern of Holzenburg et al. (1993) appear very similar to the type B crystal of Bassi et al. (1989). The type B crystal consisted of a double layer of crystals aligned to give an apparent single diffraction pattern. It is possible that the results of Holzenburg et al. (1993) can be explained by a similar alignment of two crystal layers and the resulting misleading diffraction pattern.

The calculated potential mass of the monomer in the tubular crystals was 332 kD (Table II). The potential mass of the polypeptides and pigments of a single PS II complex in the tubular crystals is 270 kD, assuming 1:1 stoichiometry of all polypeptides present (reviews, Bricker, 1990; Jansson, 1994). Thus, the unit cell has sufficient volume to include two, but not four, PS II complexes. Similar volume considerations have indicated dimeric PS II units in a

number of studies (Irrgang et al., 1988; Bassi et al., 1989; Haag et al., 1990; Boekema et al., 1994; Santini et al., 1994). The estimates of volume/mass involve certain assumptions regarding the stoichiometry of polypeptides, average densities of proteins and determination of protein boundaries. However, bearing this in mind, structural work with two-dimensional crystals or isolated particles has suggested more than sufficient volume to include two PS II units. It should be noted that there is biochemical evidence that PS II complexes found in the grana portions of thylakoids are dimeric (Peter and Thornber, 1991; Santini et al., 1994), suggesting that dimeric PS II complexes are in fact the functional unit.

Structure: Interpretation of the Densities

One of the advantages of determining the structure of protein crystals in ice is the visualization of that portion of the protein embedded in the membrane (Milligan et al., 1984). In an earlier projection map of negatively stained PS II crystals, there were four main areas of density (Lyon et al., 1993). The projection map of the frozen hydrated PS II dimer shows an expanded shape and more discernible densities due to the integral membrane portions of the complex (Fig. 4 *a*). Because the topography has changed, new nomenclature was necessary. Further discussion will utilize the nomenclature outlined in the Results section and shown in Fig. 4 *b*.

For the first time, it is possible to associate densities in the projection map of PS II with specific polypeptides. Labeling with F_{ab} fragments against the D1 and the cyt b559 (alpha subunit) polypeptides places both proteins in the same density, region A. The close association of D1 and cyt b559 is in clear agreement with the results of Nanba and Satoh (1987), who isolated the minimum components for PS II photochemical activity. These minimum components were D1, D2, and cyt b559, implying that these three
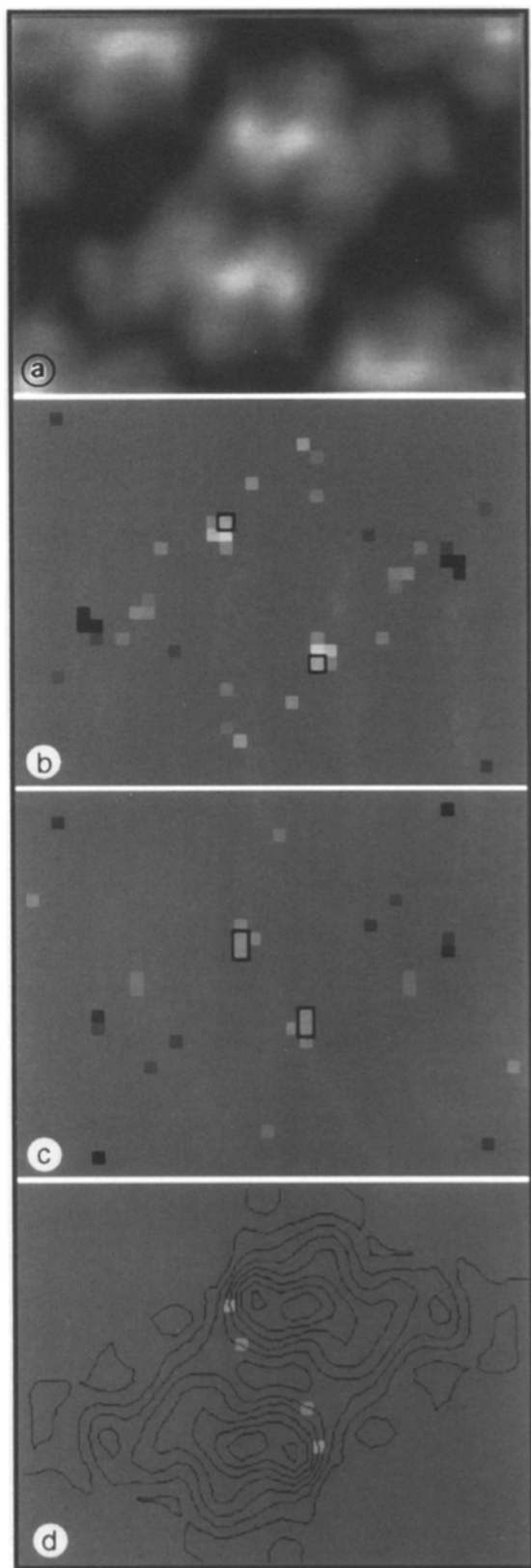
were in close proximity to one another. The antibodies used were generated using synthetic polypeptides from the COOH terminus of each sequence. Therefore, the locations of the label indicate the locations of the COOH termini of each protein. In the tubular crystals, the lumenal side of the PS II complex is exposed to the surface. Thus, the labeling results confirm earlier work that showed that the COOH termini for these proteins reside in the lumen (Sayre et al., 1986; Cramer et al., 1993).

Considering the comparison between the L and M subunits from the bacterial reaction center and the reaction center core of PS II (Holschuh et al., 1984; Zurawski et al., 1984; Deisenhofer and Michel, 1989), as well as the fact that D1, D2, and cyt b559 can be isolated readily as a functional unit (Nanba and Satoh, 1987), it is likely that the D2 polypeptide is also located near region A. CP47 also has been isolated with the core as a functional unit (Dekker et al., 1990). The two most intense densities, A and B (more striking in the negatively stained complex, Fig. 6 a), correspond to areas which extend the farthest from the membrane's surface. The CP47 sequence predicts that CP47 has several loops which extend from the membrane (review, Bricker, 1990). In addition, CP47 is the largest polypeptide in the complex and would therefore contribute greatly to the density. Furthermore, there is evidence that CP47 and cyt b559 are in close proximity (Picorel et al., 1994), suggesting that cyt b559 is located near both CP47 and D1-D2. Thus, it is likely that CP47 is located in the regions A and B. The rest of the monomer must contain the remaining antennae proteins. CP43 has been isolated with CP47 and the core as a functional unit (Ghanotakis et al., 1987; Fotinou et al., 1993). Consequently, CP43 is likely to be closely associated with these polypeptides. CP29, CP26, CP24, and CP22 are mostly buried in the membrane, based on sequence homology with LHC II, (Green and Pickersky, 1994) whose structure is known to atomic resolution (Kühlbrandt et al., 1994). They may be located primarily in the regions of low density which are more visible in ice. There is some evidence that these antennae polypeptides do not have 1:1 stoichiometry with the core components (Bassi and Dainese, 1992). There was a subtle difference between the two halves of the dimer in the low density areas, which may reflect a slightly different complement of antennae polypeptides for each half of the dimer.

In summary, the reaction center cores are located in a position that is near the central cleft of the dimer, yet at the same time exposed to the outer edge of the dimer. In this location, the D1 polypeptide would be readily accessible for replacement after damage caused by photoinhibition (for review see Aro et al., 1993). Within the monomer, the core is surrounded on two sides by regions of low density, presumably the PS II antennae polypeptides. Noting that one of these low density areas, region D, has close proximity to the core on the opposing half of the dimer, there may be sharing of antennae functions between the

Figure 6. (*a*) Projection map of single unit cell; the map is an average from a control grid and has been filtered to 2.0 nm resolution, with twofold symmetry imposed. (*b*) Differences between the D1 labeled and control grand averages that are significant at the 0.05 level. The boxed pixel has $P = 0.0027$. (*c*) Differences between the cyt b559 labeled and the control grand averages that

are significant at the 0.05 level. The boxed pixels have $P = 0.007$ and 0.0038. (*d*) Contour map derived from the control PS II complex with the locations of the most significant differences from D1 and cyt b559 superimposed.

two halves. At the same time, the two cores are in a position to associate transiently with additional antennae and plastiquinones.

References

Aro, E.M., I. Virgin, and B. Andersson. 1993. Photoinhibition of photosystem II. Inactivation, protein damage and turnover. *Biochim. Biophys. Acta.* 1143: 113–134.

Bassi, R., and P. Dainese. 1992. A supramolecular light-harvesting complex from chloroplast photosystem II membranes. *Eur. J. Biochem.* 204:317–326.

Bassi, R., A.G. Magaldi, G. Tognon, G.M. Giacometti, and K.R. Miller. 1989. Two-dimensional crystals of the photosystem II reaction center complex from higher plants. *Eur. J. Cell Biol.* 50:84–93.

Berthold, D.A., G.T. Babcock, and C.F. Yocum. 1981. A highly resolved oxygen-evolving photosystem II preparation from spinach thylakoid membranes. *Biochim. Biophys. Acta.* 764:179–183.

Boekema, E.J., A.F. Boonstra, J.P. Dekker, and M. Rogner. 1994. Electron microscopic structural analysis of photosystem I, photosystem II and the cytochrome b6/f complex from green plants and cyanobacteria. *J. Bioenerg. Biomembr.* 26:17–29.

Boekema, E.J., B. Hankamer, D. Bald, J. Kruip, J. Nield, A. Boonstra, J. Barber, and M. Rögner. 1995. Supramolecular structure of the photosystem II complex from green plants and cyanobacteria. *Proc. Natl. Acad. Sci. USA.* 92:175–179.

Bowlby, N.R., and C.F. Yocum. 1993. Effects of cholate on Photosystem II: selective extraction of a 22 kDa polypeptide and modification of Q_b-site activity. *Biochim. Biophys. Acta.* 1144:271–277.

Bricker, T.M. 1990. The structure and function of CPa-1 and CPa-2 in photosystem II. *Photosynth. Res.* 24:1–13.

Brisson, A., and P.N.T. Unwin. 1985. Quaternary structure of the acetylcholine receptor. *Nature (Lond.).* 315:474–477.

Cramer, W.A., G.-S. Tae, P.N. Furbacher, and M. Bottger. 1993. The enigmatic cytochrome b-559 of oxygenic photosynthesis. *Physiol. Plant.* 88:705–711.

Deisenhofer, J., and H. Michel. 1989. The photosynthetic reaction center from the purple bacterium *Rhodopseudomonas virids*. *EMBO (Eur. Mol. Biol. Organ.) J.* 8:2149–2169.

Dekker, J.P., S.D. Betts, C.F. Yocum, and E.J. Boekema. 1990. Characterization by electron microscopy of isolated particles and two-dimensional crystals of the CP47-D1-D2-cytochrome b-559 complex of photosystem II. *Biochemistry.* 29:3220–3225.

Falbel, T.G., and L.A. Staehelin. 1992. Species-related differences in the electrophoretic behavior of CP29 and CP26 : an immunochemical analysis. *Photosynth. Res.* 34:249–262.

Fotinou, C., M. Kokkinidis, G. Fritzsch, W. Haase, H. Michel, and D.F. Ghanotakis. 1993. Characterization of a photosystem II core and its three-dimensional crystals. *Photosynth. Res.* 37:41–48.

Frank, J., and W. Goldfarb. 1980. Methods for averaging of single molecules and lattice-fragments. *In* Electron Microscopy at Molecular Dimensions. W. Baumeister, and W. Vogell, editors. Springer-Verlag, Heidelberg. 261–269.

Frank, J., B. Shimkin, and H. Dowse. 1981. SPIDER: a modular software system for electron image processing. *Ultramicroscopy.* 6:343–358.

Ghanotakis, D.F., and C.F. Yocum. 1990. Photosystem II and the oxygen-evolving complex. *Annu. Rev. Plant Physiol. Plant Mol. Biol.* 41:255–276.

Ghanotakis, D.F., D.M. Demetriou, and C.F. Yocum. 1987. Isolation and characterization of an oxygen evolving PSII reaction center core preparation and a 28 kDa chla binding protein. *Biochim. Biophys. Acta.* 891:15–21.

Gounaris, K., D. Whitford, and J. Barber. 1983. The effect of thylakoid lipids on an oxygen-evolving photosystem II preparation. *FEBS Lett.* 163:230–234.

Green, B.R., and E. Pichersky. 1994. Hypothesis for the evolution of three helix Chl a/b and Chl a/c light harvesting antennae proteins from two-helix and four-helix ancestors. *Photosyn. Res.* 39:149–162.

Guo, X.W., P.R. Smith, B. Cognon, D. D'Arcangelis, and E. Dolginova. 1995. Molecular design of the voltage dependent, anion-selective channel in the mitochondrial outer membrane. *J. Struc. Biol.* 114:41–59.

Haag, E., K.-D. Irrgang, E.J. Boekema, and G. Renger. 1990. Functional and

structural analysis of photosystem II core complexes from spinach with high oxygen evolution capacity. *Eur. J. Biochem.* 189:47–53.

Hansson, O., and T. Wydrzynski. 1990. Current perceptions of photosystem II. *Photosynth. Res.* 23:131–162.

Holschuh, K., W. Bottomley, and P.R. Whitfield. 1984. Structure of the spinach chloroplast genes for the D2 and 44 kd reaction-center proteins of photosystem II and for tRNA ser(UGA). *Nucleic Acid Res.* 12:8819–8834.

Holzenburg, A., M.C. Bewley, F.H. Wilson, W.V. Nicholson, and R.C. Ford. 1993. Three-dimensional structure of photosystem II. *Nature (Lond.).* 363: 470–472.

Høyer-Hansen, G., R. Bassi, L.S. Honberg, and D.J. Simpson. 1988. Immunological characterization of chlorophyll a/b binding proteins of barley thylakoids. *Planta.* 173:12–21.

Ikeuchi, M., and Y. Inoue. 1988. A new photosystem II reaction center component (4.8 kD protein) encoded by the chloroplast genome. *FEBS Lett.* 241: 99–104.

Irrgang, K.D., E.J. Boekema, J. Vater, and G. Renger. 1988. Structural determination of the photosystem II core complex from spinach. *Eur. J. Biochem.* 178:209–217.

Jacob, J.S., and K.R. Miller. 1986. The effects of galactolipid depletion on the structure of a photosynthetic membrane. *J. Cell Biol.* 103:1337–1347.

Jansson, S. 1994. The light-harvesting chlorophyll a/b binding proteins. *Biochim. Biophys. Acta.* 1184:1–19.

Kates, M. 1972. Techniques of Lipidology: Isolation, Analysis and Identification of Lipids. North-Holland Publishing Company, Amsterdam. 544–551.

Kubalek, E., S. Ralston, J. Lindstrom, and N. Unwin. 1987. Location of subunits within the acetylcholine receptor by electron image analysis of tubular crystals from *Torpedo marmorata. J. Cell Biol.* 105:9–18.

Kühlbrandt, W. 1987. Photosynthetic membranes and membrane proteins. *In* Electron Microscopy of Proteins. Vol. 6: Membraneous Structures. J.R. Harris, and R.W. Horne, editors. Academic Press, London. 155–207.

Kühlbrandt, W., D.N. Wang, and Y. Fujiyoshi. 1994. Atomic model of plant light-harvesting complex by electron crystallography. *Nature (Lond.).* 367: 614–621.

Ljungberg, U., H.-E. Åkerlund, and B. Andersson. 1986. Isolation and characterization of the 10-kDa and 22-kDa polypeptides of higher plant photosystem 2. *Eur. J. Biochem.* 158:477–482.

Lyon, M.K., K.M. Marr, and P.S. Furcinitti. 1993. Formation and characterization of two-dimensional crystals of photosystem II. *J. Structur. Biol.* 110:133–140.

Mastronarde, D.N., E.T. O'Toole, K.L. McDonald, J.R. McIntosh, and M.E. Porter. 1992. Arrangement of inner dynein arms in wild-type and mutant flagella of Chlamydamonas. *J. Cell Biol.* 118:1145–1162.

Mastronarde, D.N., K.L. McDonald, R. Ding, and J.R. McIntosh. 1993. Interpolar spindle microtubules in PTK cells. *J. Cell Biol.* 123:1475–1489.

Miller, K.R., and J.S. Jacob. 1991. Surface structure of the photosystem II complex. *In* EMSA Proceedings. G.W. Bailey, and E.L. Hall, editors. San Francisco Press, San Francisco. 196–197.

Milligan, R.A., A. Brisson, and P.N.T. Unwin. 1984. Molecular structure determination of crystalline specimens in frozen aqueous solutions. *Ultramicroscopy.* 13:1–10.

Murphy, D.J. 1986. The molecular organization of the photosynthetic membranes of higher plants. *Biochim. Biophys. Acta.* 864:33–94.

Nanba, O., and K. Satoh. 1987. Isolation of a photosystem II reaction center consisting of D1 and D2 polypeptides and cytochrome b559. *Proc. Natl. Acad. Sci. USA.* 84:109–112.

Nixon, P.J., J.G. Metz, M. Rogner, and B.A. Diner. 1990. A *Synechocystis* PCC 6803 psbA deletion mutant and its transformation with a psbA gene from a higher plant. *In* Current Research in Photosynthesis. M. Baltscheffsky, editor. Kluwer Academic Press, Dordrecht, Netherlands. Vol. I:471–474.

Peter, G.F., and J.P. Thornber. 1991. Biochemical evidence that the higher plant photosystem II core complex is organized as a dimer. *Plant Cell Physiol.* 32:1237–1250.

Picorel, R., G. Chumanov, T.M. Cotton, G. Montoya, S. Toon, and M. Seibert. 1994. Surface-enhanced resonance Raman scattering spectroscopy of photosystem II pigment-protein complexes. *J. Phys. Chem.* 98:6017–6022.

Press, W.H., B.P. Flannery, S.A. Teukolsky, and W.T. Vetterling. 1989. Numerical Recipes: The Art of Scientific Computing. Cambridge University Press, Cambridge. 818 pp.

Rawyler, A., and P.A. Siegenthaler. 1980. Rapid analysis of membrane lipids using a combination of thin-layer chromatography and scanning of photographic negatives. *J. Biochem. Biophys. Methods.* 2:271–281.

Santini, C., V. Tidu, G. Tognon, A.G. Magaldi, and R. Bassi. 1994. Three-dimensional structure of the higher-plant photosystem II reaction centre and evidence for its dimeric organization *in vivo. Eur. J. Biochem.* 221:307–315.

Saxton, W.O., and W. Baumeister. 1982. The correlation averaging of a regularly arranged bacterial envelope protein. *J. Microsc. (Oxf.)* 127:127–138.

Sayre, R.T., B. Andersson, and L. Bogorad. 1986. The topology of a membrane protein: the orientation of the 32 kd Qb-binding chloroplast thylakoid membrane protein. *Cell.* 21:601–608.

Schroder, W.P., T. Henrysson, and H.E. Åkerlund. 1988. Characterization of low molecular mass proteins of photosystem II by N-terminal sequencing. *FEBS Lett.* 235:289–292.

Seibert, M., M. DeWitt, and L.A. Staehelin. 1987. Multimeric (tetrameric) particles on the lumenal surface of freeze-etched photosynthetic membranes. *J.*

Cell Biol. 105:2257–2265.

Siegenthaler, P.-A., J. Smutny, and A. Rawyler. 1987. Involvement of distinct populations of phosphatidylglycerol and phosphotidylcholine molecules in photosynthetic electron-flow activities. *Biochim. Biophys. Acta.* 891:85–93.

Simpson, D.J. 1983. Freeze-fracture studies on barley plastid membranes. VI. Location of the P700-chlorophyll a-protein 1. *Eur. J. Cell Biol.* 31:305–314.

Simpson, D., and B. Andersson. 1986. Extrinsic polypeptides of the chloroplast oxygen evolving complex constitute the tetrameric ESs particles of higher plant thylakoids. *Carlsberg Res. Commun.* 51:467–474.

Sokal, R.R., and F.J. Rohlf. 1981. Biometry. 2nd ed. W.H. Freeman, New York. 859 pp.

Staehelin, L.A., and G.W.M. Van der Staay. 1996. Structure, composition, functional organization and dynamic properties of thylakoid membranes. *In* Oxygenic Photosynthesis: The Light Reactions. D.R. Ort and C.F. Yocum, editors. Kluwer Academic Publishers, the Netherlands. In press.

Tae, G.-S., M.T. Black, W.A. Cramer, O. Vallon, and L. Bogorad. 1988. Thyla-

koid membrane protein topography: transmembrane orientation of the chloroplast cytochrome b-559 psbE gene product. *Biochemistry.* 27:9075–9080.

Unser, M., B.L. Trus, and A.C. Steven. 1987. A new resolution criterion based on the spectral signal-to-noise ratio. *Ultramicroscopy.* 23:39–52.

Walpole, R.E., and R.H. Myers. 1978. Probability and Statistics for Engineers and Scientists. 2nd ed. MacMillan Publishing Co., Inc. NY. 249–256.

Wand, M.P., and M.C. Jones. 1995. Kernel Smoothing. Chapman and Hall, London. 212 pp.

Zhou, Z.H., and W. Chiu. 1993. Prospects for using an IVEM with a FEG for imaging macromolecules toward atomic resolution. *Ultramicroscopy.* 49: 407–416.

Zurawski, G., H.J. Bohnert, P.R. Whitfield, and W. Bottomley. 1984. Nucleotide sequence of the gene for Mr 32,000 thylakoid membrane protein from *Spinacia oleracea* and *Nicotiana debneyi* of Mr 38,950. *Proc. Natl. Acad. Sci. USA.* 79:7699–7703.